2010 IEEE International Conference on Robotics and Automation
Anchorage Convention District
May 3-8, 2010, Anchorage, Alaska, USA

Optimizing Coordinate Choice for Locomoting Systems

Ross L. Hatton and Howie Choset
{rlhatton, choset}@cmu.edu

Abstract— **Gait evaluation techniques that use Stokes's theorem to integrate a system's equations of motion have traditionally been limited to finding only the net rotations or small translations produced by gaits. Recently, we have observed that certain choices of generalized coordinates allow these techniques to be extended to gaits that produce large translations. In this paper, we present a method for finding the optimal coordinate choice for this purpose, based on a Hodge-Helmholtz decomposition of the system constraints, and demonstrate the efficacy of the Stokes's theorem approach over a wide variety of gaits when using the optimized coordinate choice.**

I. Introduction

Conventional geometric treatments of locomotion have been relatively agnostic with regard to the choice of generalized coordinates they use. If any consideration is given to this choice, it is generally for the purpose of simplifying the expression of system constraints or dynamics. Our recent results [1] have shown that an appropriate coordinate choice can also simplify motion planning and gait design. In this paper, we explore means for optimally making this coordinate choice.

Our work builds on the body of locomotion literature which uses geometric mechanics to separate internal shape changes from the external motions they produce. The application of geometric mechanics to locomotion, pioneered by Shapere and Wilczek [2] and further developed by Murray and Sastry [3] and Kelly and Murray [4], provides a powerful mathematical framework for analyzing locomotion. A key product of this work is the development of the *reconstruction equation* and *local connection* for nonholonomic systems, which relate body velocity to changes in internal shape for a broad class of locomoting systems. We will not rederive the reconstruction equation here; for a thorough treatment, see [5]–[7].

This reconstruction equation has been used in a variety of locomotion contexts. Ostrowski *et al.* [6], [8] combined the reconstruction equation with Lie bracket theory to generate sinusoidal gaits which translate and rotate a variety of snake-like systems. Bullo and Lynch used the reconstruction equation to decouple the locomotion of kinodynamic systems and design kinematic gaits [9]. More recently, there has been interest in applying these techniques to swimming robots, such as McIsaac and Ostrowski's work on anguilliform (eel-like) robots [10] and Morgansen *et al.*'s work on fish [11], both of which combine the geometric approach with biomimetic elements. In [12], we introduced the *connection vector field* as a tool for visualizing the reconstruction equation differentially, and thus gaining intuition on systems' kinematics.

It is not generally possible to integrate the reconstruction equation in closed form, raising difficulties for the inverse problem of finding shape changes which result in desired translations. In special cases, however, Stokes's theorem can be used to find the net motion resulting from gaits [4]. Mukherjee [13] used this principle to analyze the motion of rolling disks, and Walsh and Sastry [14] applied it to the case of an isolated three-link robot. Shammas *et al.* [7], [15] combined this approach with the reconstruction equation to define functions on the shape space of their three-link robots which allowed the design of gaits resulting in specified rotations. A similar technique was used by Melli *et al.* [16] and later by Avron and Raz [17] to generate gaits for swimming robots. In [1], we first identified the importance of coordinate choice in applying these methods to approximating the net translation produced by gaits, and used a mean-orientation coordinate choice to extend the Stokes's theorem results to the design of translational gaits.

Here, we advance the consideration of coordinate choice to include a notion of *optimal coordinates* which allow the displacement over the widest variety of gaits to be approximated via Stokes's theorem. We first identify the space of available generalized coordinate choices for the problem. From within this space, we then relate the optimal coordinates to a minimization of the norm of the local connection, which we achieve via a modification of the Hodge-Helmholtz decomposition [18]. To demonstrate the efficacy of this change of coordinates, we evaluate a large selection of gaits for which the Stokes's theorem approximation is within ten percent of the actual displacement.

II. Background

While the principles we are investigating are relevant to a wide range of systems, including fish, differential drive cars, and satellites, in this paper we focus on a particular system, the *three-link kinematic snake* investigated by Shammas *et al.* [7], [15]. Illustrated in Fig. 1, this system has a passive wheelset on each link, preventing lateral translation while freely allowing rotation and longitudinal translation. The kinematic snake's configuration is a combination of its shape $r = (\alpha_1, \alpha_2)$ and position and orientation $g = (x, y, \theta)$. The *body velocity*, ξ, of the system is its position velocity in the x^b and y^b directions and the angular velocity of the (x^b, y^b) frame.

As detailed in [7], the kinematic snake's shape and body velocities are related in the *kinematic reconstruction equation*,

$$\xi = -\mathbf{A}(r)\dot{r}, \tag{1}$$

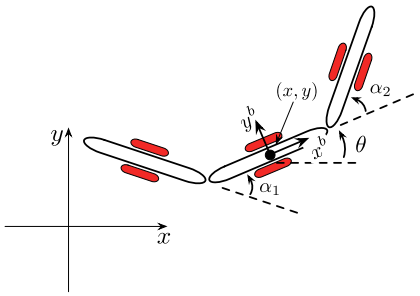

Fig. 1: Model for the three-link kinematic snake. The overall location of the system is the x, y position and orientation θ of the middle link with respect to the fixed coordinate system. The shape coordinates are α_1 and α_2, the angles of the two joints. The passive wheels on each link constrain lateral but not longitudinal or rotational motion.

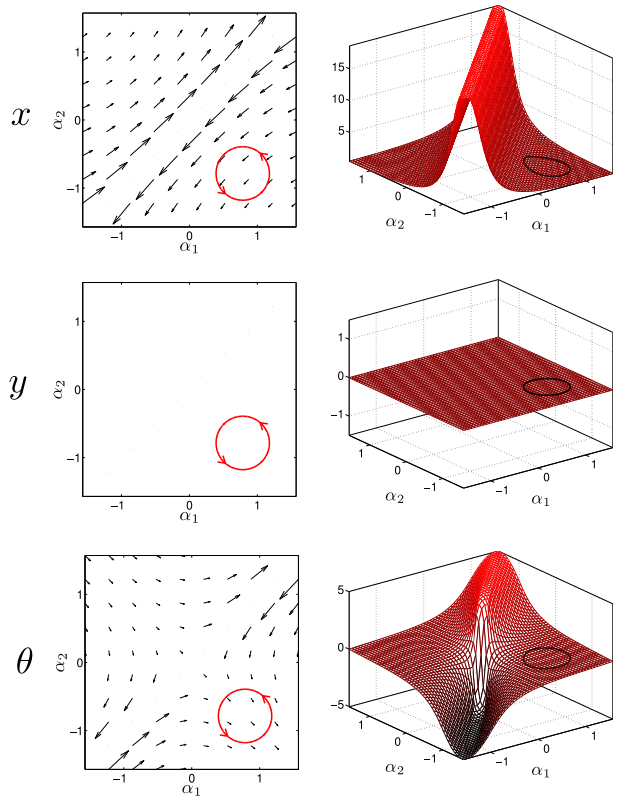

Fig. 2: Representative gait image-family overlaid on the connection vector fields and height functions of the kinematic snake in the coordinate system depicted in Fig. 1. (Because of singularities in the local connection, the magnitudes of the height functions and vector fields are scaled by an arctangent function.)

by the *local connection*, $\mathbf{A}$, which acts as a Jacobian in body coordinates. To visualize the structure of the local connection, we separate out the rows of $-\mathbf{A}$ into *connection vector fields* [12], which represent the local gradients of the components of g with respect to the shape; these fields are plotted for the kinematic snake in the first column of Fig. 2.

In motion planning for locomoting systems like the kinematic snake, we are especially interested in evaluating the net displacement over *gaits*, or cyclic repeatable shape changes. As in [1], we regard a gait as a closed trajectory in the shape space with a specific starting point; a *gait image-family* is the collection of all gaits tracing out the same closed curve.

The displacement over a gait is found by integrating

$$g(t) = \int_0^t \begin{bmatrix} \cos\theta(\tau) & -\sin\theta(\tau) & 0 \\ \sin\theta(\tau) & \cos\theta(\tau) & 0 \\ 0 & 0 & 1 \end{bmatrix} \begin{bmatrix} \xi_x(\tau) \\ \xi_y(\tau) \\ \xi_\theta(\tau) \end{bmatrix} d\tau, \quad (2)$$

where the body velocity is rotated into global coordinates at each time. A second quantity of motion over a gait is the *body velocity integral* (BVI) [1], which measures the "forwards minus backwards" motion in each body direction, and is the simple vector integral of the body velocity,

$$\zeta(t) = \begin{bmatrix} \zeta_x(t) \\ \zeta_y(t) \\ \zeta_\theta(t) \end{bmatrix} = \int_0^t \begin{bmatrix} \xi_x(\tau) \\ \xi_y(\tau) \\ \xi_\theta(\tau) \end{bmatrix} d\tau. \quad (3)$$

This quantity can be conveniently calculated via Stokes's theorem as the area integral of the curls of the connection vector fields (plotted as height functions in the second column of Fig. 2) over the area enclosed by the gait. While the BVI is in general not a useful indication of the net displacement over a gait, we observed in [1] that we can interpret the BVI as an approximation of the displacement, with error

$$\varepsilon_\zeta = \zeta - g = \int_0^t \begin{bmatrix} 1-\cos\theta & \sin\theta & 0 \\ -\sin\theta & 1-\cos\theta & 0 \\ 0 & 0 & 0 \end{bmatrix} \begin{bmatrix} \xi_x \\ \xi_y \\ \xi_\theta \end{bmatrix} d\tau. \quad (4)$$

We further observed that for gaits in regions of the shape space where $\vec{\mathbf{A}}^{\xi_\theta}$ vanishes, $\dot{\theta}$, θ, and ε_ζ must all be small, making the BVI a good approximation of the displacement. Finally, we showed that we can manipulate the connection vector fields and generate near-null regions of $\vec{\mathbf{A}}^{\xi_\theta}$ by appropriately choosing the parameterization of the systems. As a demonstration, we recalculated the local connection with θ as the mean orientation of the three links, rather than the orientation of the middle link; for this choice of coordinates, the BVI for the gaits in the example image-family approximated the displacements with an error of less than 5%, as opposed to a 67% error using the original orientation.

III. Valid Coordinate Choices

The utility of the connection height functions in the mean-orientation coordinate system raises two important questions: First, what properties of the mean-orientation coordinate system led to the improvement? Second, what other coordinate sets are available, and might they provide even more nullification of the $\vec{\mathbf{A}}^{\xi_\theta}$ field? Starting with the second question, we put forward the notion of a *valid coordinate set* as one which induces a body frame for which the body velocity is produced by a reconstruction equation of the form in (1). This notion is compatible with the derivations of the reconstruction equation in [4], [7], [19], which also include means of testing the validity of individual coordinate sets. The test used in those works is, unfortunately, only useful for validating given coordinate sets, and do not provide a means for finding new coordinate sets except by trial and error. However, if we have a valid coordinate set from which to

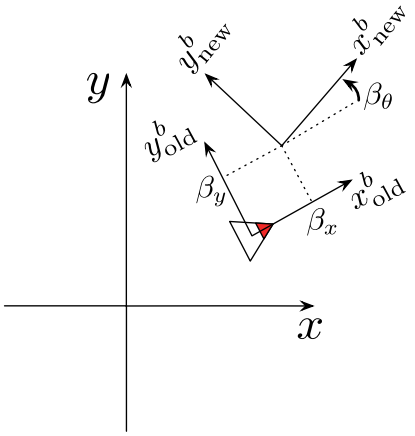

Fig. 3: An original, known-valid body frame, and a new frame displaced from that frame by β

start, such as that in Fig. 1, we can use the following lemma to directly find other valid coordinate sets.

Lemma 3.1 (Relationship of valid coordinate sets): In any valid coordinate set (*i.e.*, one for which a local connection can be derived), the body frame of the system described by the coordinates is related by a shape-dependent transform $\beta(r)$ to the body frame in a coordinate set known to be valid.

Proof: Consider the two coordinate frames shown in Fig. 3. The frame designated by $(x^b_{\text{old}}, y^b_{\text{old}})$ represents an original, known-valid body frame for the system and the frame designated by $(x^b_{\text{new}}, y^b_{\text{new}})$ is a second frame which is a candidate to be a body frame under a new choice of coordinates. For any such frame, we can define its position and orientation in the original body frame to be $\beta = (\beta_x, \beta_y, \beta_\theta)$, as shown in Fig. 3. The body velocity ξ^{new} of this frame, *i.e.*, its velocity as measured along its own instantaneous coordinates, is

$$\xi^{\text{new}} = B_{\text{rot}} \cdot (\xi + \dot{\beta} + B_\times \xi_\theta), \tag{5}$$

where $\dot{\beta}$ represents the relative velocity of the two frames as measured in the original frame, $B_\times$ is the cross product term which gives the translational velocity of the velocity of the new frame produced by rotation of the old frame,

$$B_\times = \begin{bmatrix} -\beta_y & \beta_x & 0 \end{bmatrix}^T, \tag{6}$$

and B_{rot} is the rotation matrix

$$B_{\text{rot}} = \begin{bmatrix} \cos\beta_\theta & \sin\beta_\theta & 0 \\ -\sin\beta_\theta & \cos\beta_\theta & 0 \\ 0 & 0 & 1 \end{bmatrix} \tag{7}$$

which handles the conversion of the velocity vector between the two frames.

For the kinematic systems we are considering, if this new frame is a valid body frame for the system, then ξ^{new} must be produced by a kinematic reconstruction equation of the form in (1). For new frames in which β is a function of r, the relative velocity between the frames is

$$\dot{\beta} = \frac{\partial \beta}{\partial r}\dot{r} \tag{8}$$

and the cross product term is also a function of the shape, so (5) thus becomes

$$\xi^{\text{new}} = B_{\text{rot}}(r) \cdot (\xi + \frac{\partial \beta}{\partial r}\dot{r} + B_\times(r)\xi_\theta). \tag{9}$$

By substituting in the original kinematic reconstruction equation (1) into (9) and regrouping,

$$\begin{aligned} \xi^{\text{new}} &= B_{\text{rot}}(r) \cdot (-\mathbf{A}(r)\dot{r} + \frac{\partial \beta}{\partial r}\dot{r} - B_\times(r)\mathbf{A}^{\xi_\theta}(r)\dot{r}) && (10)\\ &= B_{\text{rot}}(r) \cdot (-\mathbf{A}(r) + \frac{\partial \beta}{\partial r} - B_\times(r)\mathbf{A}^{\xi_\theta}(r))\dot{r} && (11)\\ &= -\mathbf{A}_{\text{new}}(r)\dot{r}, && (12) \end{aligned}$$

we see that ξ^{new} is produced by a matrix of the right form to be a local connection, and that having β as a function of r is sufficient to define a valid body frame. To see that it is also a necessary condition, consider the effect of defining β as a function of anything other than r. In this situation, the expansion of (5) into (9) would contain terms that cannot be collected into $\mathbf{A}_{\text{new}}(r)$ in (12), precluding such a β from meeting our definition of a valid coordinate system.

□

IV. Finding an Optimal Coordinate Choice

Having defined the valid body frames, and thus the available choices of coordinates, we can address the questions of why the mean orientation body frame was a good choice and how to systematically find an optimal choice.

A. Optimal Choice of Orientation

The key to finding the optimal choice of orientation lies in the third row of the $\frac{\partial \beta}{\partial r}$ term in (9), $\frac{\partial \beta_\theta}{\partial r}$. As β_θ is a function of r, $\frac{\partial \beta_\theta}{\partial r}$ is its gradient with respect to the shape, $\nabla\beta_\theta$. Because B_{rot} and $B_\times$ only contribute to the translational components of the new local connection, any difference between $\vec{\mathbf{A}}^{\xi_\theta}$ and $\vec{\mathbf{A}}^{\xi_\theta}_{\text{new}}$ is due to the addition of $\nabla\beta_\theta$.

When moving from the center-link frame for the kinematic snake to the mean orientation frame, $\beta_\theta = (-\alpha_1 + \alpha_2)/3$ and its gradient is $\nabla\beta_\theta = \begin{bmatrix} -\frac{1}{3} & \frac{1}{3} \end{bmatrix}$. Figure 4 visually represents the addition of this gradient field to the original $\vec{\mathbf{A}}^{\xi_\theta}$ field. In the two circled regions, the fields cancel each other out, creating null regions of $\vec{\mathbf{A}}^{\xi_\theta}_{\text{new}}$. In these regions, the new body frame counterrotates with respect to the center-link frame, and thus rotates very little with respect to the world in response to shape changes. *Consequently, the BVI closely approximates the displacement for gaits in these regions*

Based on this observation of what makes the mean-orientation frame an effective choice of coordinates, we now have a criterion for an optimal choice of coordinates: It should induce a $\nabla\beta_\theta$ field that most nullifies $\vec{\mathbf{A}}^{\xi_\theta}$.[1] While the exact meaning of "most nullifies" is open to interpretation, for now we will take it as a minimization of the average

[1]Note the necessary condition from Lemma 3.1 that β be a function only of r, which in turn restricts the selection of the nullifying field to be from the set of gradient fields on the shape space.

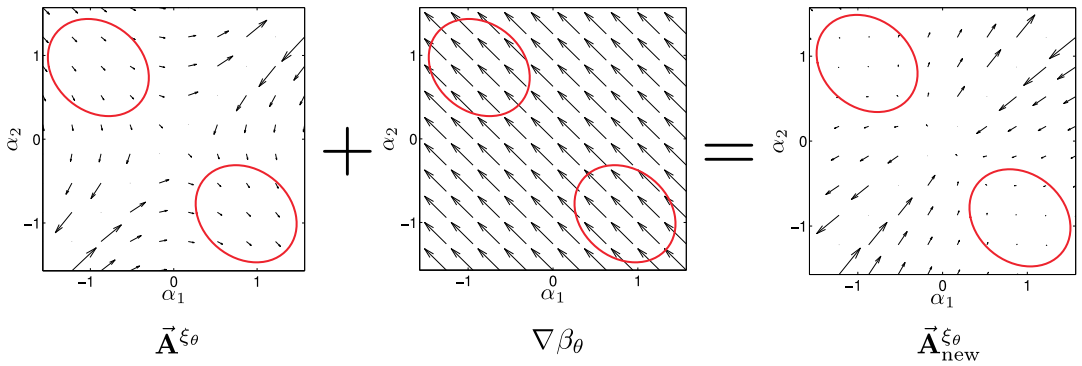

Fig. 4: The effect of adding $\nabla\beta_\theta$ for the mean orientation coordinate choice to $\vec{\mathbf{A}}^{\xi_\theta}$. In the circled regions, $\nabla\beta_\theta \approx -\vec{\mathbf{A}}^{\xi_\theta}(r)$, so $\|\vec{\mathbf{A}}^{\xi_\theta}_{\text{new}}\| \approx 0$ in these regions. Note that for visual clarity within each plot, the vectors in the different fields are not to scale.

squared magnitude $\vec{\mathbf{A}}^{\xi_\theta}_{\text{new}}$ over the region of interest, *i.e.*, minimizing D for

$$D = \iint_\Omega \|\vec{\mathbf{A}}^{\xi_\theta} + \nabla\beta_\theta\|^2 \, d\Omega \tag{13}$$

for $\Omega \subset M$. Because β_θ is a function of r, we can generate it directly from $\nabla\beta_\theta$ (modulo an integration constant) and we can shift attention to directly finding $\nabla\beta_\theta$ that minimizes (13).

Identifying optimal coordinate choices with minimizations of D in (13) provides the key to finding the best coordinate choices for arbitrary systems. The cost function D is minimized when $\nabla\beta_\theta$ is the gradient field which most closely approximates $-\vec{\mathbf{A}}^{\xi_\theta}$, *i.e.*, is the negative projection of $\vec{\mathbf{A}}^{\xi_\theta}$ onto the space of conservative vector fields. This projection is identical to the *Hodge-Helmholtz Decomposition* [18], which separates a vector field into a conservative component and a divergence-free remainder. Here, the conservative component is equal to $-\nabla\beta_\theta$, while the remainder becomes $\vec{\mathbf{A}}^{\xi_\theta}_{\text{new}}$.

While an analytical solution for this projection requires that $\vec{\mathbf{A}}^{\xi_\theta}$ meet certain regularity conditions and is not generally feasible, the *Discrete Hodge-Helmholtz Decomposition* [20] provides a numerical minimization of (13). This decomposition is relatively easy to compute for arbitrary vector fields via finite element methods, by restricting β_θ to the class of weighted sums of basis functions ϕ, $\beta_\theta = \sum_i \phi_i e_i$, and applying the necessary condition $\partial D/\partial e_i = 0 \; \forall \; i$ at the minimum of D to convert (13) into

$$\int_\Omega \nabla\phi_i \cdot \nabla\beta_\theta \, d\Omega = \int_\Omega \nabla\phi_i \cdot \vec{\mathbf{A}}^{\xi_\theta} \, d\Omega, \tag{14}$$

which, on a discretized grid, can be solved as a set of linear equations for the weights e as detailed in [20].

In practice, we have found that an extra refinement to the decomposition is necessary when $\vec{\mathbf{A}}^{\xi_\theta}$ has singularities. The large magnitudes of such fields in the vicinity of the singularities dominate the integral in (13), producing a $\nabla\beta_\theta$ field that closely approximates $-\vec{\mathbf{A}}^{\xi_\theta}$ at the singularities, but at the expense of any accuracy over the rest of the field. We address this limitation by using the same arctangent scaling we use to display the vector fields, and instead solve the minimization problem

$$D = \iint_\Omega \left\| \frac{\arctan(k\|\vec{\mathbf{A}}^{\xi_\theta}\|)}{k\|\vec{\mathbf{A}}^{\xi_\theta}\|} \vec{\mathbf{A}}^{\xi_\theta} + \nabla\beta_\theta \right\|^2 d\Omega, \tag{15}$$

where the scaling factor $k = 0.2/\text{median}(\|\vec{\mathbf{A}}^{\xi_\theta}\|)$ modifies the arctangent function such that the center of its linear region corresponds to the median value of the range of input vector magnitudes. The arctangent scaling acts as a selective weighting function that emphasizes the quality of the fit in the low-control-force regions of the shape space, away from the singularities.

B. Optimal Choice of Reference Position

While the choices of β_x and β_y do not affect the magnitude of $\vec{\mathbf{A}}^{\xi_\theta}$, they do contribute to the goal of minimizing the error between the BVI and the displacement. Returning to (4), we observe that the rotation matrix term is multiplied by the translational body velocity, $[\xi_x \; \xi_y]^T$. It therefore follows that minimizing this body velocity by choosing a coordinate system that minimizes $\vec{\mathbf{A}}^{\xi_x}$ and $\vec{\mathbf{A}}^{\xi_y}$ will further reduce the error beyond the reduction already accomplished by an optimal choice of β_θ.

Finding the optimal choice of position coordinates has a similar formulation to finding the optimal choice of orientation, in that we are looking for a change of coordinates which most nullifies the translational connection vector fields. The key difference from the orientation optimization lies in the $B_\times$ term, which is now non-zero. Beyond adding a third term into the summations of vector fields that produce $\vec{\mathbf{A}}^{\xi_x}_{\text{new}}$ and $\vec{\mathbf{A}}^{\xi_y}_{\text{new}}$, $B_\times$ also couples these two calculations, so we must simultaneously solve for β_x and β_y to minimize D in

$$D = \iint_\Omega \|\vec{\mathbf{A}}^{\xi_x} + \nabla\beta_x - \beta_y\vec{\mathbf{A}}^{\xi_\theta}\|^2 + \|\vec{\mathbf{A}}^{\xi_y} + \nabla\beta_y + \beta_x\vec{\mathbf{A}}^{\xi_\theta}\|^2 \, d\Omega. \tag{16}$$

As with the Discrete Hodge-Helmholtz Decomposition, we take a finite element approach to this minimization, taking $\beta_x = \sum_i \phi_i e_i$ and $\beta_y = \sum_i \phi_i f_i$ and applying the minimization conditions $\partial D/\partial e_i = 0$ and $\partial D/\partial f_i = 0$ to generate

the equated integrals

$$\int_\Omega \nabla\phi_i \cdot (\nabla\beta_x - \beta_y \vec{\mathbf{A}}^{\xi_\theta}) + \phi_i(\beta_x \vec{\mathbf{A}}^{\xi_\theta} + \nabla\beta_y)\, d\Omega$$
$$= \int_\Omega \nabla\phi_i \cdot (-\vec{\mathbf{A}}^{\xi_x}) - \phi_i(\vec{\mathbf{A}}^{\xi_y} \cdot \vec{\mathbf{A}}^{\xi_\theta})\, d\Omega \quad (17)$$

and

$$\int_\Omega \nabla\phi_i \cdot (\nabla\beta_y + \beta_x \vec{\mathbf{A}}^{\xi_\theta}) + \phi_i(\beta_y \vec{\mathbf{A}}^{\xi_\theta} - \nabla\beta_x)\, d\Omega$$
$$= \int_\Omega \nabla\phi_i \cdot (-\vec{\mathbf{A}}^{\xi_y}) + \phi_i(\vec{\mathbf{A}}^{\xi_y} \cdot \vec{\mathbf{A}}^{\xi_\theta})\, d\Omega. \quad (18)$$

As in the orientation optimization, we discretize these integrals on a grid and solve them as a set of linear equations for the weights e and f. Additionally, when singularities are present, we make use of the arctangent scaling approach in (15) to emphasize the regions of the shape space away from the singularities. Note that $\vec{\mathbf{A}}^{\xi_\theta}$ in this equation is for the original choice of coordinates, and that B_{rot} does not appear in the optimization as it does not affect the magnitude of the connection vector fields.

C. Summary of Coordinate Optimization

In summary, the coordinate optimization process is as follows. First, we use the Hodge-Helmholtz decomposition to find the $\nabla\beta_\theta$ field that minimizes $\vec{\mathbf{A}}^{\xi_\theta}$. Second, we integrate this field to find $\beta_\theta(r)$, choosing the integration constant so $\beta_\theta(0,0) = 0$; from β_θ, we generate the B_{rot} operator which converts the x and y components of the body velocity into the new frame. Third, solving the coupled optimization problem in (16) provides us with $\nabla\beta_x$, $\nabla\beta_y$ and $B_\times$, as plotted in Fig. 5. Finally, we insert these terms into (11) to generate the new, optimized local connection plotted in Fig. 6.

V. Results

In the optimized coordinate system, the BVI for the example gait image-family approximates the net displacement with a maximum error of less than one percent, measured as the maximum distance from the BVI to the locus of displacements divided by the minimum magnitude of displacement in the locus. As illustrated in Fig. 7, this is an improvement over the already useful approximation using the mean-orientation coordinates of [1]. The quality of the approximation is not limited to the example gaits. Figure 8 plots the maximum radii of circular image-families for which the maximum error is less than ten percent, showing effectively complete coverage of the region of the shape space for which $\vec{\mathbf{A}}^{\xi_\theta}$ is nullified in Fig. 6. This region is also an inherently good region in which to search for efficient translation gaits, as its distance from the singularities in the constraints means that gaits contained therein require low control forces.

VI. Conclusions

By identifying the space of available generalized coordinates and systematically optimizing the coordinate choice for the three-link kinematic snake, we have generalized and improved upon our results in [1]. This optimized approach

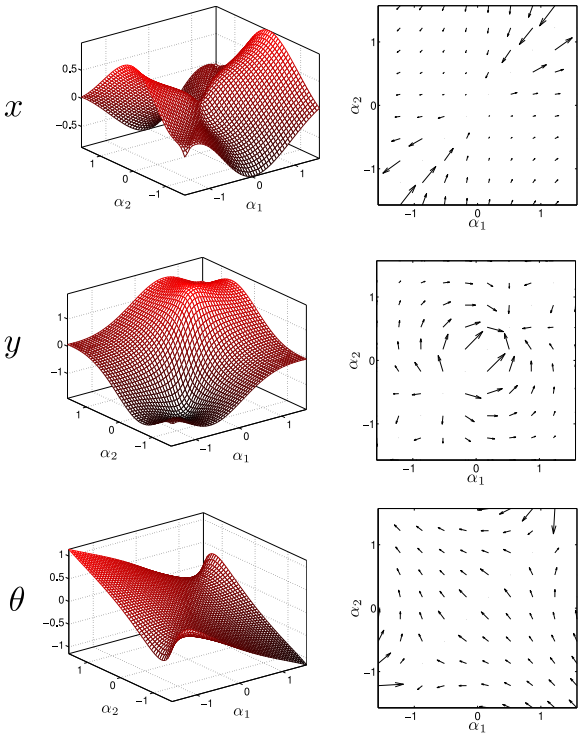

Fig. 5: Optimal β (left) and $\nabla\beta$ (right) for the kinematic snake, using the arctangent metric in (15).

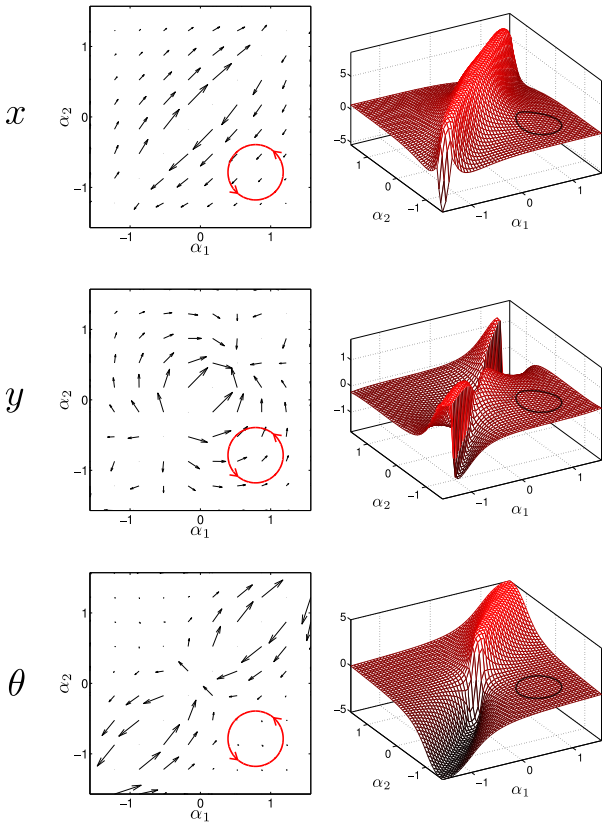

Fig. 6: Representative gait image-family overlaid on the connection vector fields and height functions of the kinematic snake in the optimized coordinate system. As compared to the mean-orientation coordinate system in [1], $\vec{\mathbf{A}}^{\xi_\theta}$ is nullified over a larger area, and $\mathbf{H}^{\zeta_y}$ shows more variation. Because of singularities in the local connection, the magnitudes of the height functions and vector fields are scaled to their arctangents.

requires no intuition about the physical characteristics of the system and can be applied automatically based on the structure of the local connection, making it easily extendable to other systems, including the swimming systems in [16], [17]. Our future work in this area will investigate such applications, along with developing optimization techniques that take advantage of the height functions to efficiently generate gaits producing desired net displacements.

REFERENCES

[1] R. L. Hatton and H. Choset, "Approximating Displacement with the Body Velocity Integral," in *Proceedings of Robotics: Science and Systems*, Seattle, USA, June 2009.

[2] A. Shapere and F. Wilczek, "Geometry of Self-Propulsion at Low Reynolds Number," *Geometric Phases in Physics*, Jan 1989.

[3] R. Murray and S. Sastry, "Nonholonomic Motion Planning: Steering Using Sinusoids," *IEEE Transactions on Automatic Control*, Jan 1993. [Online]. Available: http://eavr.u-strasbg.fr/~bernard/education/ensps_3a/tmp/murray.pdf

[4] S. Kelly and R. M. Murray, "Geometric Phases and Robotic Locomotion," *J. Robotic Systems*, Jan 1995. [Online]. Available: ftp://avalon.caltech.edu/pub/murray/preprints/cds/cds94-014.ps.gz

[5] A. M. Bloch *et al.*, *Nonholonomic Mechanics and Control*. Springer, 2003.

[6] J. Ostrowski and J. Burdick, "The Mechanics and Control of Undulatory Locomotion," *International Journal of Robotics Research*, vol. 17, no. 7, pp. 683 – 701, July 1998.

[7] E. A. Shammas, H. Choset, and A. A. Rizzi, "Geometric Motion Planning Analysis for Two Classes of Underactuated Mechanical Systems," *The International Journal of Robotics Research*, vol. 26, no. 10, pp. 1043–1073, 2007. [Online]. Available: http://ijr.sagepub.com/cgi/content/abstract/26/10/1043

[8] J. Ostrowski, J. Desai, and V. Kumar, "Optimal Gait Selection for Nonholonomic Locomotion Systems," *International Journal of Robotics Research*, 2000.

[9] F. Bullo and K. M. Lynch, "Kinematic Controllability for Decoupled Trajectory Planning in Underactuated Mechanical Systems," *IEEE Transactions on Robotics and Automation*, vol. 17, no. 4, pp. 402–412, August 2001.

[10] K. McIsaac and J. P. Ostrowski, "Motion Planning for Anguilliform Locomotion," *Robotics and Automation*, Jan 2003. [Online]. Available: http://ieeexplore.ieee.org/xpls/abs_all.jsp?arnumber=1220714

[11] K. Morgansen, B. Triplett, and D. Klein, "Geometric Methods for Modeling and Control of Free-Swimming Fin-Actuated Underwater Vehicles," *Robotics*, Jan 2007. [Online]. Available: http://ieeexplore.ieee.org/xpls/abs_all.jsp?arnumber=4399955

[12] R. L. Hatton and H. Choset, "Connection Vector Fields for Underactuated Systems," *IEEE BioRob*, October 2008.

[13] R. Mukherjee and D. Anderson, "Nonholonomic Motion Planning Using Stokes' Theorem," in *IEEE International Conference on Robotics and Automation*, 1993.

[14] G. Walsh and S. Sastry, "On Reorienting Linked Rigid Bodies Using Internal Motions," *Robotics and Automation, IEEE Transactions on*, vol. 11, no. 1, pp. 139–146, January 1995.

[15] E. Shammas, K. Schmidt, and H. Choset, "Natural Gait Generation Techniques for Multi-bodied Isolated Mechanical Systems," in *IEEE International Conference on Robotics and Automation*, 2005.

[16] J. B. Melli, C. W. Rowley, and D. S. Rufat, "Motion Planning for an Articulated Body in a Perfect Planar Fluid," *SIAM Journal of Applied Dynamical Systems*, vol. 5, no. 4, pp. 650–669, November 2006.

[17] J. Avron and O. Raz, "A Geometric Theory of Swimming: Purcell's Swimmer and its Symmetrized Cousin," *New Journal of Physics*, 2008.

[18] G. B. Arfken, *Mathematical Methods for Physicists*, 6th ed. Elsevier, 2005.

[19] J. Ostrowski, "Reduced Equations for Nonholonomic Mechanical Systems with Dissipation," *Journal of Mathematical Physics*, 1998.

[20] Q. Guo, M. K. Mandal, and M. Y. Li, "Efficient Hodge-Helmholtz Decomposition of Motion Fields," *Pattern Recognition Letters*, vol. 26, no. 4, pp. 493–501, 2005.

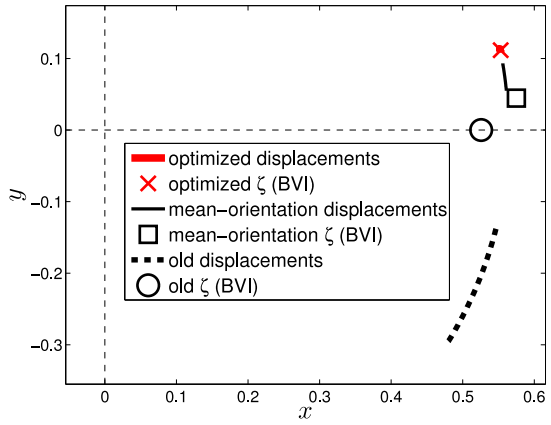

Fig. 7: The BVI and displacements corresponding to the image-family of gaits in Fig. 6 for the kinematic snake robot with the optimized measure of orientation from Fig. 5 are represented respectively by the cross above the x-axis and a very short arc section at the same location, with the BVI and displacements as measured in the original and mean-orientation coordinate choices presented for reference.

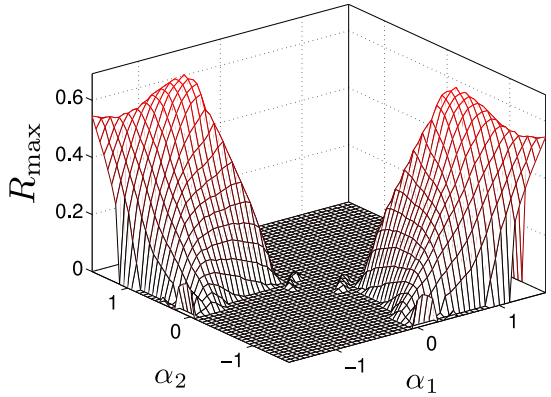

(a)

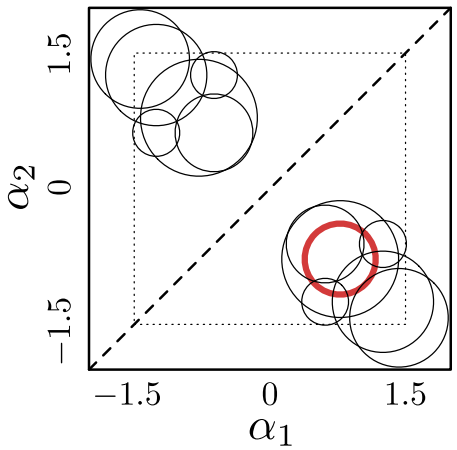

(b)

Fig. 8: Maximum radius of for a circular gait image-family for less than ten percent BVI error, (a) plotted as a function on the shape space, and (b) drawn as a representative collection of image-families. In (b), the dashed line denotes the $\alpha_1 = \alpha_2$ singularity and the dotted box marks the extent of the domain of the plot in (a). The thick-lined circle in the lower-right portion of the drawing is the gait image-family used in the main examples.